AIMS Materials Science, 3(2): 470-485.
DOI: 10.3934/matersci.2016.2.470
Received: 26 February 2016
Accepted: 06 April 2016
Published: 08 April 2016

http://www.aimspress.com/journal/Materials

Research article

Development of low temperature technology for the growth of wide band gap semiconductor nanowires

David Jishiashvili *, Zeinab Shiolashvili, Archil Chirakadze, Alexander Jishiashvili, Nino Makhatadze, and Kakha Gorgadze

Institute of Cybernetics, Georgian Technical University, 77 Kostava St., 0175, Tbilisi, Georgia

* **Correspondence:** Email: d_jishiashvili@gtu.ge.

Abstract: $In_2Ge_2O_7$, Ge_3N_4, In_2O_3 and germanium nanowires were synthesized by the developed hydrazine (N_2H_4)-based technology. Annealing of germanium or Ge+In sources in the vapor of N_2H_4+3 mol.% H_2O caused the formation of volatile GeO and In_2O molecules in the hot zone. These molecules were transferred to the Si substrate, which was placed in the could zone of a reactor. After interacting with hydrazine decomposition products (NH_3, NH_2, NH, H_2, H) and water, Ge_3N_4 nanowires and nanobelts were produced on the Ge source in the temperature range of 500–520 ºC. The growth temperature of Ge_3N_4 nanowires in hydrazine vapor was by 350 ºC lower than the temperature reported in the literature. Using In+Ge source the tapered In_2O_3 nanowires were formed on the Si substrate at 400 ºC. At 420–440 ºC the mixture of In_2O_3 and Ge nanowires were synthesized, while at 450 ºC $In_2Ge_2O_7$ nanowires were produced, with InN nanocrystals growing on their stems. The possible chemical reactions for the synthesis of these nanostructures were evaluated. The growth temperatures of both, $In_2Ge_2O_7$ and InN nanostructures were by 50–150 ºC lower than that, reported in the literature. The results of this work clearly demonstrate the ability of hydrazine vapor to reduce the growth temperature of nitride and oxide nanomaterials.

Keywords: nanowires; $In_2Ge_2O_7$; Ge_3N_4; I_2O_3; hydrazine; InN

1. Introduction

The modern concept of environment protection is based on the continuous monitoring of air, soil, water pollution and permanent control of solar radiation that reaches the earth surface. The growth of ozone hole results in higher doses of Ultra Violet (UV) irradiation and increases the

demand for sensitive UV photodetectors, which can distinguish the real UV signal from solar background radiation. In the widely used Si UV detectors, this problem is solved by utilizing Wood's optical filters, which complicates its design and increases the cost. In contrast to this, the UV detectors based on Wide Band Gap (WBG) semiconductors with energy gaps higher then ~4.5 eV have an intrinsic solar blindness as they are insensitive to sunlight with energies less than the ban gap value [1–4]. Such UV detectors are of utmost importance also for the space and sun exploration, flame analysis, missile tracking systems, space flight security, photocatalytic CO_2 reduction, chemical and biological analysis, power electronics, electric vehicles, high energy lasers etc. [5–8].

Indium germinate - $In_2Ge_2O_7$, with the band gap of E_g = 4.3 eV, is a promising and valuable material not only for luminescent devices [8,9], sensors [10] and thermoelectric generators [11,12], but also for solar-blind UV photodetectors. Due to very low dark current, such detectors can work not only without optical cut-off filters, but also without heavy cooling systems [3,4,13].

Group III nitrides (AlN and GaN) and their ternary and quaternary compounds with each other and InN, are considered to be the most promising WBG materials for the development of high-performance devices, including UV photodetectors. They have many advantages such as the ideal spectral selectivity with wide direct band gaps from the deep UV to the infrared region, high breakdown field, high thermal and chemical stability, radiation hardness and expected high responsivity. However, formation of stoichiometric single crystalline nitrides is a complicated task, which was solved for GaN by Nakamura, Akasaki and Amano (2014 Nobel Prize in physics) after ~20 years of technological investigation. Indium nitride with low defect concentration was produced only in the beginning of this century and its true band gap value was established to be ~0.7 eV.

The development of new, effective methods for the synthesis of nitride materials is an important technological issue and the objective of this paper addresses this challenge.

The application of one dimensional (1D) nanostructures instead of thin films and bulk materials have significantly improved the performance of devices due to the unique surface related and quantum confinement features, together with an increased light absorption and ability to realize axial and radial homo- and hetero- p-n junction within a single nanowire. The growth temperature of such nanomaterials should be kept sufficiently low to prevent the formation of thermal stresses in the substrate, redistribution of impurities and degradation of p-n junctions. From the other hand, the growth technology should utilize highly active precursors to provide formation of stoichiometric and structurally perfect nanomaterials. It should be also taken into account that the structure and morphology of NWs can be greatly influenced by the source materials and precursor species [14,15,16].

In this paper, we describe the development of low temperature growth technology for producing oxide and nitride wide band gap semiconductor 1D nanostructures ($In_2Ge_2O_7$ E_g = 4.3 eV, Ge_3N_4 E_g = 3.9 eV). The technology is based on the application of active gaseous precursors formed after thermal decomposition of hydrazine vapor. One purpose of this work was also to investigate the nature of precursors and chemical processes that provide the growth of 1D nanostructures in hydrazine vapor.

2. Materials and Method

The growth of nanowires was performed in the glass vacuum system with 50 mm diameter vertical quartz reactor. The small ampoule with hydrazine was connected with the reactor through the

glass valve. The temperature of hydrazine was kept close to 20 ºC. The system was evacuated down to 2×10^{-5} Torr using a rotary and glass diffusion pumps. The external resistive furnace (400W) was attached to the bottom of the reactor. Its temperature was controlled by k-type thermocouple. The hydrazine–hydrate was purified by distillation and the water content in it was evaluated using the refractometer. The details of technology and precursor formation are considered in the following section.

The morphology and structure of NWs were studied using FEI Quanta FEG 600 Scanning Electron Microscope (SEM) and Philips CM200 FEG Transmission Electron Microscope (TEM). XRD data were taken on a Shimadzu XRD-6000 diffractometer.

3. Results and Discussion

3.1. Formation of precursor for the growth of nanowires

The low temperature facile synthesis of nitride materials needs the application of spontaneous chemical reactions with negative Gibbs free energies and high kinetic factors. Nitrogen molecule with its very hard triple bond is useless for nitride formation unless it is dissociated or ionized to form atomic nitrogen or N^+ ion. The utilization of ammonia lowers the synthetic temperature, however, it is still sufficiently high with average value close to 1000 ºC.

Hydrazine (N_2H_4) based technology attracted our attention because in the early work of S.Vashioka [17] it was reported that the rate of Si_3N_4 film deposition in hydrazine was increased by 50 times as compared with the synthesis in ammonia. This was explained by a high concentration of active NH_2 radicals in the products formed after thermal decomposition of hydrazine. Besides, it was established that at the surfaces of semiconductors the decomposition of hydrazine proceeds as a very fast chain reaction with a high pre-exponential factor of $10^{13}s^{-1}$ [18]. In spite of these advantages the application of hydrazine vapor and its flows for producing microelectronic materials and nanostructures was not popular due to the explosive nature and toxicity of N_2H_4. From the other hand, different very active radicals (NH_2,NH, atomic nitrogen and hydrogen) are produced during the pyrolysis of hydrazine, until the final stabile products – N_2, H_2 and NH_3 are formed [19,20,21]. These radicals offer a special opportunity to decrease the synthetic temperature of different materials including nano-dimensional structures, as discussed in the following sections.

It should be noted that after purification of hydrazine hydrate, approximately 3mol.% of water still remained in the hydrazine and served as oxidants for producing volatile suboxides. Considering the gas phase precursors formed after thermal decomposition of N_2H_4 + 3mol.%H_2O it becomes clear that reducing, oxidizing and nitride forming species are simultaneously presented in the reactor. This leads to the variety of competitive paths for the chemical synthesis of nanomaterials. Depending on the source material and process temperature different pure materials and compounds can be produced including oxides, nitrides and oxinitrides. In our previous work we used a piece of crystalline InP as a source and demonstrated that in hydrazine vapor pure, crystalline InP nanowires can be synthesized on Si substrate, despite the presence of oxidizing and nitride forming precursors [22]. The possible reason lies in the very high value of negative Gibbs free energy (−904 kJ/mol at 400 ºC) and increased kinetic factor for the chemical reaction that produces InP from In_2O and P precursors, instead of Indium oxide or nitride formation. In the considered process of InP nanowire growth,

oxygen manifests itself only in producing volatile In_2O soboxides that provide the indium mass transfer to Si substrate.

In this work we used crystalline, unpolished, solid Ge and In sources for producing nanowires. The only possible volatile species, which are able to perform the mass transfer from source to substrate and subsequent growth of nanowires are volatile GeO and In_2O suboxides. In our oxygen deficient atmosphere they can be produced onto the source surfaces after dissociative adsorption of water molecules or after reduction of existing native oxide layers with H_2, H, NH and NH_2 species.

The experimental setup with vertical, tubular quartz reactor was first evaporated down to 2×10^{-5} Torr, then isolated from the vacuum system and filled with hydrazine vapor up to its saturated pressure of ~10 Torr. The solid source material was placed on the bottom of the reactor (hot zone) and heated by an external resistive furnace. The substrate (Si and glass) were placed on a tubular quartz spacer at 3–20mm above the source (cold zone) and heated by the convective heat transfer from the same furnace. The temperature of the substrates was regulated by changing the source-substrate distance.

3.2. Growth of Ge_3N_4 nanowires from Ge source

For the growth of Ge_3N_4 nanowires the Ge source was placed on the bottom of a reactor and Si substrate was located at 3 mm above it. The source was annealed in hydrazine vapor for 1 hour in the temperature range of 400–550 ºC, and the corresponding substrate temperature range was 380–530 ºC.

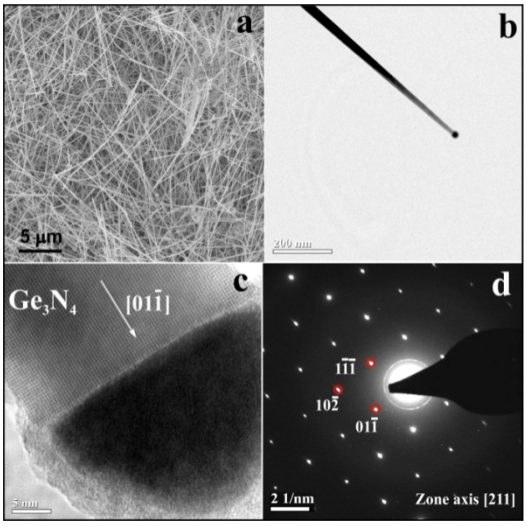

Figure 1. SEM (a) and TEM images (b,c) of nanowires grown on Ge source at 500 ºC. (d) Selected Area Electron Diffraction (SAED) pattern, which confirms the formation of α phase Ge_3N_4 nanowire.

It should be emphasized that during the growth process Ge_3N_4 nanowires were produced both on source and Si substrate surfaces. However, their morphologies, composition and growth mechanisms were quite different. In our previous work [23] we presented some results concerning the growth of Ge_3N_4 nanowires on the surface of Ge source without considering the growth processes

at the Si substrate surface, which was placed above the source. It was established that the first step in the growth of NWs on Ge source is a formation of GeO_x clusters, followed by the appearance of molten Ge self catalyst droplets. At 500 ºC α-Ge_3N_4 nanowires started to grow on Ge source surface. They were produced through the self-catalyzed Vapor-Liquid-Solid (VLS) mechanism using GeO vapor and nitride forming precursors, produced after pyrolytic decomposition of hydrazine. The minimum diameter of nanowires was 7 nm, while their lengths exceeded tens of micrometers. Figure 1 represents SEM and TEM images of Ge_3N_4 nanowires. They confirm the Ge catalyst-assisted growth of single crystalline α-Ge_3N_4 nanowires. It should be noted that Ge catalyst was also successfully used for producing different nanowires including SiO_2, Al_2O_3, ZnO, GaN [24–27].

At elevated temperatures close to 520 ºC the growth mechanism was changed to Vapor-Solid one and α-Ge_3N_4 nanobelts were produced instead of nanowires with circular diameters (Figure 2). Some of them had thicknesses close to few atomic layers, while their lengths reach tens of micrometers.

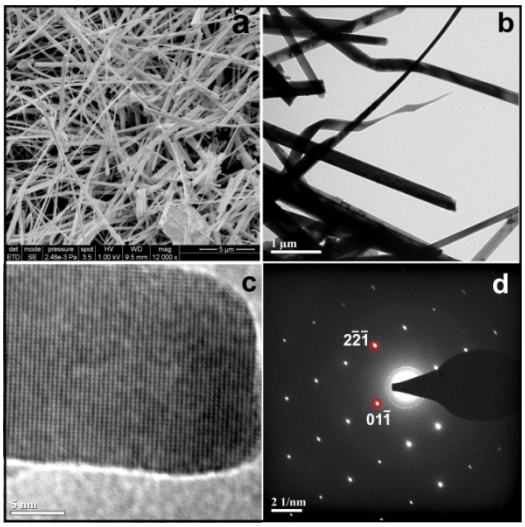

Figure 2. SEM (a) and TEM images (b,c) of α- Ge_3N_4 nanobelts formed at 520 ºC on the surface of Ge source. (d) corresponding SAED pattern.

The morphology of grown 1D nanostructures strongly depended on the growth temperature. At higher temperatures close to 580 ºC the large, micrometer sized crystalline blocks of Ge_3N_4 were produced, however, they still preserved the elongated shapes (Figure 3).

More detailed information about precursors, their activity and chemical reactions involved in the synthesis of nanowires were obtained after analysis of nanomaterials produced during the condensation of GeO molecules on the Si substrate and their interaction with hydrazine decomposition products. The elemental mappings of nanomaterials synthesized on Si surface at different temperatures are presented below in Figures 4–6.

The microdroplets and linear, chain-like structures were observed in material grown at 480 ºC. The whole product consisted mainly of Ge (Figure 4 b). The formation of germanium nitride or oxide was not observed (Figure 4 c,d), indicating that GeO vapor was effectively reduced to Ge by hydrazine decomposition products. The absence of a surface covering thin film proves that the droplets and chains were formed after surface diffusion and coalescence of adatoms. The micrometer

sizes of material suggest that the flux of Ge molecules was sufficiently dense. Probably, at early stage of growth, when sizes of first clusters were within few nanometers, they were molten nanodroplets due to well known Gibbs-Thomson effect. As the sizes grew, the temperature was insufficient to keep them in liquid state and the spherical shape was changed to irregular one observed in Figure 4. The origin of driving force that arranges the droplets in a chain-like structure is unknown. XRD spectra of materials that were scrapped off the Si surface did not reveal any presence of crystalline Ge. The absence of crystallites may be caused by insufficient substrate temperature, and partly by a relatively high level of oxygen and nitrogen impurities in Ge droplets.

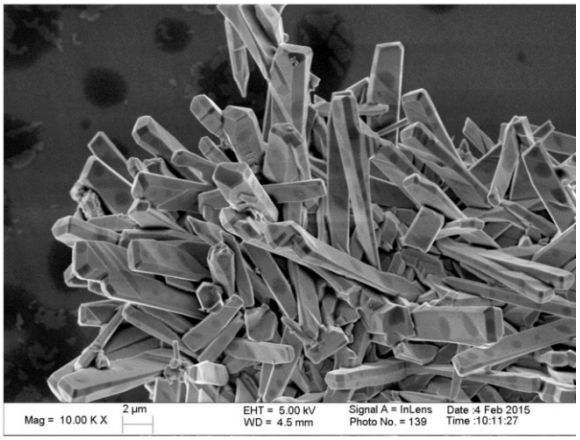

Figure 3. SEM image of α-Ge_3N_4 crystalline blocks, formed at Ge source surface at 580 ºC.

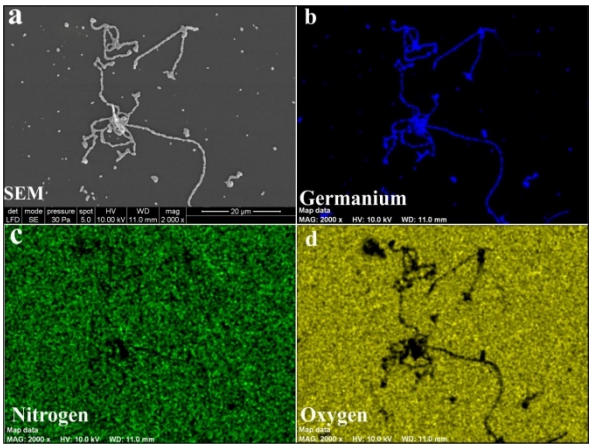

Figure 4. SEM image (a) and elemental mapping of nanomaterials produced on Si substrate at 480 ºC (b–d).

At increased temperature (500 ºC) the VLS grown Ge_3N_4 nanowires with facetted edges appear at the Si surface along with Ge chains (Figure 5). The produced 1D Ge_3N_4 structures we denote as nanowires, but in reality they are microwires because their diameters have micrometer sizes. The nanowires were grown through the Ge self-catalyzed VLS mechanism, because the tips are clearly seen in Ge related map (Figure 5b), but they disappear in nitrogen map (Figure 5c). The nanowire bodies consist of Ge and nitrogen. At this temperature the conversion of GeO molecules to Ge_3N_4

starts due to chemical reactions with nitrogen precursors. However the temperature is insufficient to transform all GeO molecules into nitride. As a result, a part of them is still reduced to Ge forming chains and droplets (Figure 5b).

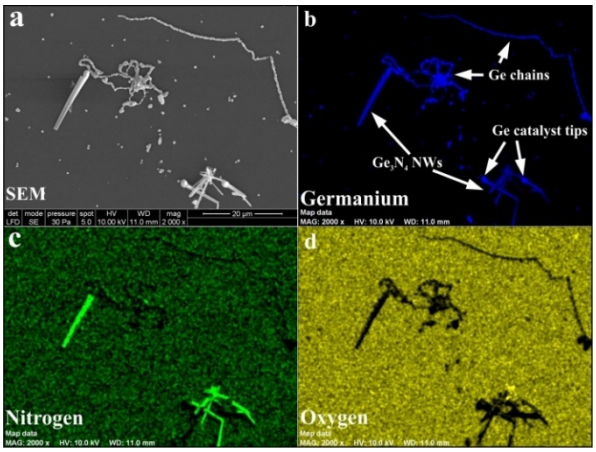

Figure 5. SEM image (a) and elemental mapping of nanomaterials produced at 500 ºC (b–d). Arrows in (b) indicate Ge_3N_4 nanowires and Ge catalyst tips. These tips are missing in nitrogen map (c).

Only germanium nitride was produced at Si surface at 520 ºC, as it is evidenced in Figure 6. No free Ge was found (Figure 6b,c). Grown nitrides have faceted edges indicating their crystalline structure. The formation of crystalline α-Ge_3N_4 phase (JCPDS: 11-69) was also confirmed by XRD pattern in Figure 6 d, which was obtained after scrapping the material off the Si substrate.

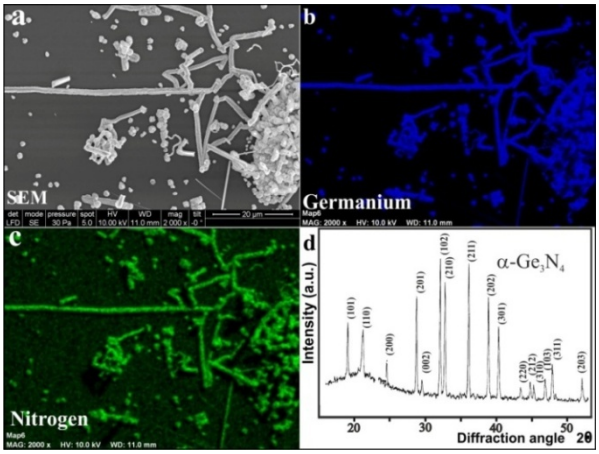

Figure 6. SEM image (a) and elemental mapping of nanomaterials produced at 520 ºC (b,c). XRD pattern of synthesized product (d).

The most striking feature of these experiments is the absence of oxides at the Si surface in spite of the presence of water and traces of O_2, which appear due to the oxygen inleakage. To explain this phenomenon we have calculated the Gibbs free energies for two sets of competitive chemical reactions. The first set was representing the processes of GeO oxidation and formation of stabile

stoichiometric GeO_2, while the second set was describing the reduction of GeO to pure Ge in hydrazine decomposition products.

Chemical reactions presented below were calculated at 500 ºC and they have a tentative nature because they were evaluated at atmospheric pressure, while the initial pressure in our experiments was 10 Torr. The sign of ΔG determines only whether or not a chemical reaction will occur. The negative signs of ΔG in the equations listed below indicate that these reactions may take place spontaneously. The real amount of synthesized material and the process dynamics depends on the reaction kinetics (i.e. on the rates of chemical processes), which were not evaluated in our experiments. However, the kinetic factors are often more important than thermodynamics in the non-equilibrium systems [28]. In these calculations GeO was considered to be in an adsorbed state.

The formation of germanium dioxide (GeO_2) through the reaction of GeO with water has a low Gibbs energy (−75 kJ/mol). The synthesis of GeO_2 through the reaction of GeO with O_2 has sufficiently higher negative free energy:

$$GeO + 0.5O_2(g) = GeO_2 \qquad \Delta G = -280 \text{ kJ/mol} \qquad (1)$$

GeO_2 can be formed also through the reaction:

$$2GeO = Ge + GeO_2 \qquad \Delta G = -218 \text{ kJ/mol} \qquad (2)$$

The Gibbs energies for the reduction of Ge from GeO using H_2 and atomic hydrogen were calculated to be −57 and −414 kJ/mol respectively.

Even more gain in energy may be obtained when Ge is reduced from GeO using NH_2 and NH species:

$$GeO + NH_{2(g)} = Ge + H_2O_{(g)} + 0.5N_{2(g)} \qquad \Delta G = -274 \text{ kJ/mol} \qquad (3)$$

$$GeO + 2NH_{(g)} = Ge + H_2O_{(g)} + N_{2(g)} \qquad \Delta G = -778 \text{ kJ/mol} \qquad (4)$$

By comparing these reactions with that of GeO_2 formation (1) and (2) it can be seen that reactions, which produce Ge are energetically mostly favorable. The considerable amount of Ge, which was synthesized on Si at 480 ºC (Figure 4) indicates that the reducing reactions have also a high kinetic factors and at this temperature they prevail over oxidation or nitride forming processes.

The syntheses of germanium nitride from existing precursors are other very favorable reactions:

$$3GeO + 4NH_{3(g)} = Ge_3N_4 + 3H_2O_{(g)} + 3H_{2(g)} \qquad \Delta G = -469 \text{ kJ/mol} \qquad (5)$$

$$3GeO + 4NH_{2(g)} = Ge_3N_4 + 3H_2O_{(g)} + H_{2(g)} \qquad \Delta G = -1196 \text{ kJ/mol} \qquad (6)$$

$$3GeO + 4NH_{(g)} + H_2(g) = Ge_3N_4 + 3H_2O_{(g)} \qquad \Delta G = -1774 \text{ kJ/mol} \qquad (7)$$

These reactions may have low kinetic factors at 480 ºC, however at 500 ºC they can proceed together with Ge reduction. As a result of these two processes the germanium chains and nitride wires may appear simultaneously and coexist at the Si surface (Figure 5). We suppose that some of small liquid Ge nanoparticles, produced at the initial stage of GeO reduction, may serve as catalyst droplets for the VLS growth of Ge_3N_4 nanowires. The nanowires are tapered with diameters increasing toward the self-catalyst tips. It is well known that the rate limiting factor in VLS growth is a process of solidification and crystal formation at the liquid catalyst - solid interface. It seems that the amount of molecules, which leave the catalyst by solidification, is lower than the amount of

gaseous molecules that enter the catalyst. This leads to the increase of catalyst diameter with time and observed tapering.

The increase of temperature up to 520 ºC causes the prevalence of reactions (5)–(7) and formation of pure germanium nitride microcrystals and crystalline 1D linear structures (Figure 6). All this material is produced through the Vapor-Solid route by direct formation of Ge_3N_4 seeds from GeO and nitrogen precursors.

It should be emphasized that there are only two publications describing the growth of Ge_3N_4 nanowires [29,30]. In both publications the synthesis was performed at 850 °C in an ammonia flow. In contrast to this, our hydrazine based technology enables the production of Ge_3N_4 nanowires at 500 ºC, which is by 350 ºC lower than that, reported in [29,30]. Besides, the Ge_3N_4 nanowires are grown without any flow of reagent gases, using only a closed vacuum system with static hydrazine pressure (~10 Torr). The presented data prove a high activity of hydrazine decomposition products and the ability to develop hydrazine based low temperature and simple technology for the growth of nitride nanowires.

3.3. Growth of nanowires from In+Ge source

As we saw in the previous section, Ge_3N_4 nanostructues were growing on both, the Ge source and Si substrate placed above it. In contrast to this, nanowires were growing only on the Si substrate when In+Ge source was used.

Some preliminary information on the composition of possible reaction products can be obtained by analyzing the thermo-chemical data of existing precursors and expected chemical reactions. The morphology and composition of nanostructures was strongly influenced by growth temperature.

When comparing indium III oxide (In_2O_3) and germanium dioxide GeO_2, it becomes clear that In_2O_3 is more stabile, as its dissociation energy per oxygen atom (466 kJ/mol) is greater than that for GeO_2 (403 kJ/mol). It means that In or In_2O will take oxygen from GeO or GeO_2 reducing them to pure Ge. The example of one of such reactions is presented below:

$$In_2O_{(g)}+2GeO=In_2O_3+2Ge \qquad \Delta G= -286 \text{ kJ/mol} \qquad (8)$$

Besides, the gaseous In_2O can readily form In III oxide through the reaction:

$$3In_2O_{(g)} =In_2O_3+4In \qquad \Delta G= -403 \text{ kJ/mol} \qquad (9)$$

The last reaction can produce pure indium droplets which may serve as sinks for In_2O_3 and arriving gaseous In_2O molecules i.e. they may serve as molten In catalysts providing the VLS growth of In_2O_3 nanowires.

Figure 7 presents tapered In_2O_3 nanowires grown on Si at 400 ºC through the VLS mechanism (source temperature 430 ºC). As it was found in the previous section, this temperature is insufficient for the effective sublimation of GeO molecules. However, the flux of In_2O molecules is quite intense because they form tapered nanowires with micrometer sized In catalyst tips. Near the bottom of nanowires, at the points where they are anchored to Si surface, their diameters are quite small and do not exceed several tens of nanometers. The diameters gradually increase towards the catalysts, reaching micrometer sizes near the tips. Some of the catalysts merge during the growth. After coalescence, a single nanowire with unified single catalyst was growing instead of two nanowires (Figure 7d).

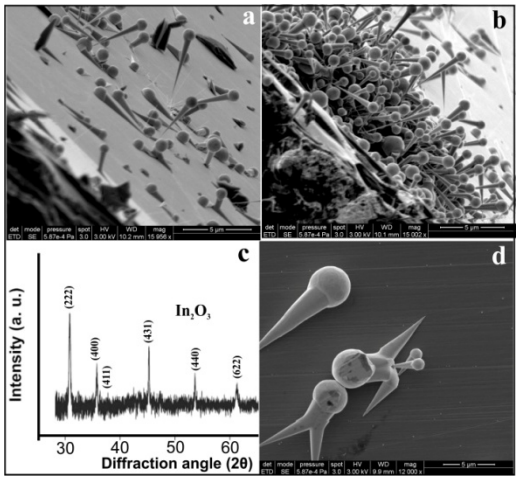

Figure 7. SEM images of In_2O_3 nanowires grown on Si substrate at 400 ºC (a,b,d). XRD pattern of nanowires (c).

The growth of In_2O_3 nanowires with indium self catalysts was proved by XRD spectrum (JCPDS: 65-3170) presented in Figure 7c. The formation of Ge or crystalline indium was not observed.

The SEM image and elemental mapping of In_2O_3 nanowires are shown in Figure 8. The spherical catalyst tips can be clearly resolved in indium related image shown in Figure 8b. However, in the same points, which are indicated by white arrows in the oxygen related map (Figure 8d), the catalysts are absent. It shows that the catalyst mainly consists of pure indium.

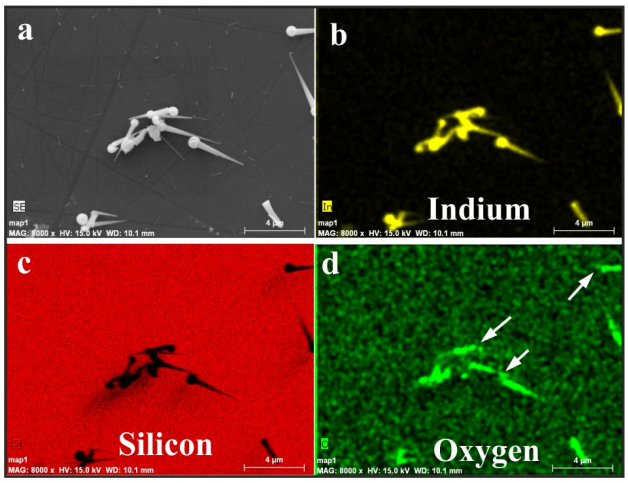

Figure 8. SEM image of In_2O_3 nanowires grown on Si substrate at 400 ºC (a). Elemental mapping of same nanowires.

The increase of substrate temperature up to 420–440 ºC causes the appearance and subsequent growth of Ge related peaks in XRD pattern (Figure 9). These peaks appear together with In_2O_3 related peaks, which are also increasing with temperature. As it was found in previous section, for the single Ge source the lowest temperature for the formation of Ge on the silicon substrate was

estimated to be 480 ºC (Figure 4). The ease of formation of crystalline Ge at 420–440 ºC in case of GeO and In_2O codeposition, can be attributed to the additional reduction of GeO through the reaction (8) and other reactions between GeO, In and In_2O precursors. As a result, at elevated temperatures the amount of reduced Ge increases in case of combined In+Ge source, in comparison with a single germanium source. The SEM image in Figure 10 demonstrates that Ge nanowires are growing through the VS process because they have no catalyst tips, while In_2O_3 nanowires are still forming by the VLS mechanism, but they are less tapered.

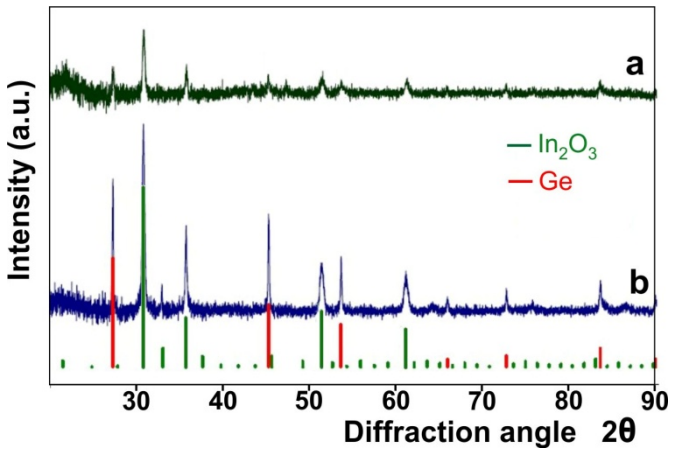

Figure 9. XRD patterns of nanowires grown from In+Ge source on Si substrate at 420 (a) and 440 ºC (b).

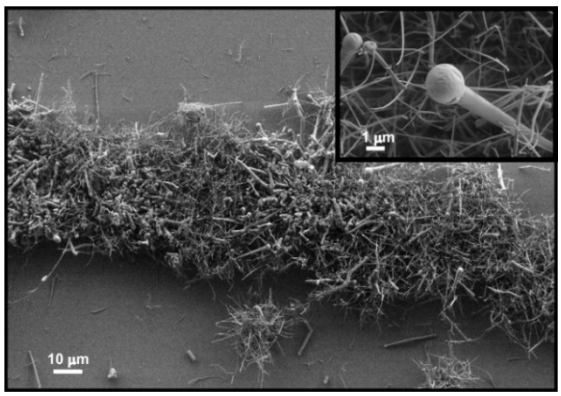

Figure 10. SEM image of Ge and In_2O_3 nanowires grown at 400 ºC. The inset shows the enlarged view of nanowires.

The whole chemistry of the growth process was changed when the substrate temperature reached 450 ºC. The nanowires grown at this temperature were scrapped off the substrate and analyzed using powder XRD technique. The pure monoclinic $In_2Ge_2O_7$ (JCPDS: 82-0846) and wurtzite InN (JCRDS: 50-1239) phases were the only crystalline materials that were detected on XRD pattern (Figure 11). TEM and SEM images of $In_2Ge_2O_7$ nanowires with attached InN nanocristals are shown in Figure 12. The selected area electron diffractions confirm the synthesis of monoclinic $In_2Ge_2O_7$ and wurtzite InN (Figure 12b,c).

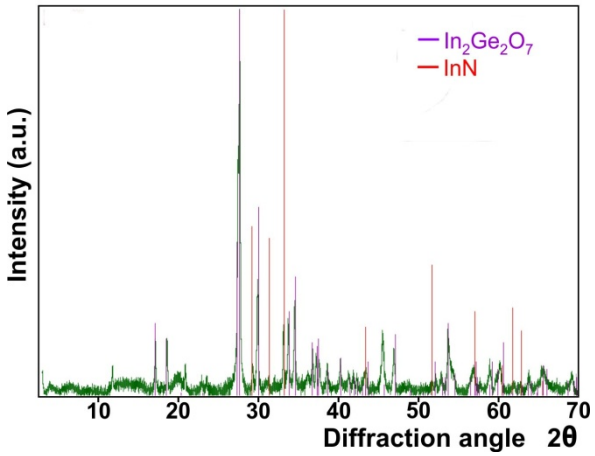

Figure 11. XRD pattern of nanowires formed on Si substrate from In+Ge source at 450 ºC.

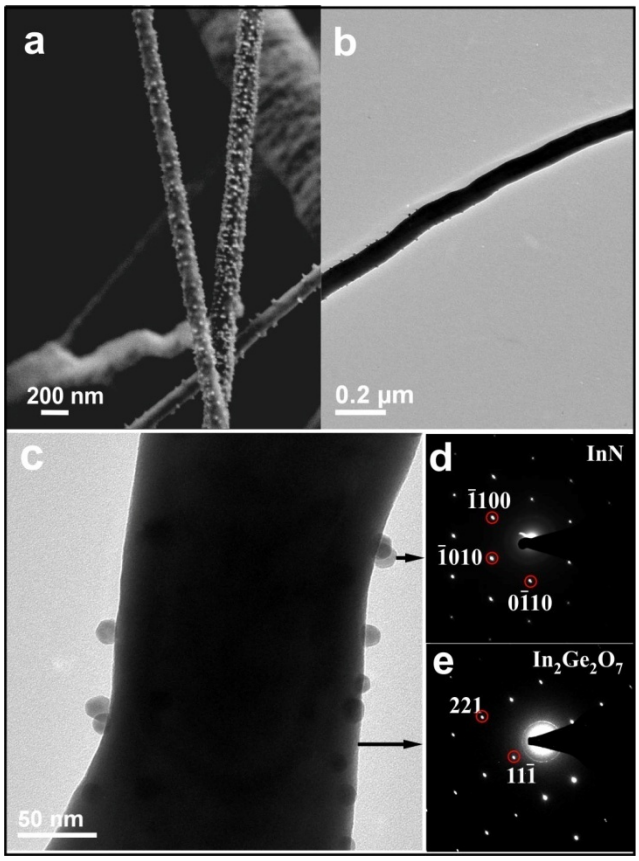

Figure 12. SEM (a) and TEM images of $In_2Ge_2O_7$ nanowire with InN nanocrystals growing on it at 450 ºC (b,c). SAED of InN nanocrystalas (d) and $In_2Ge_2O_7$ nanowire (e).

The formation of indium nitride in hydrazine-based technology is thermodynamically favorable, because the reactions of In_2O with N_2H_4 decomposition products (ammonia, NH_2 and NH) have negative Gibbs energies, with a highest value of $\Delta G = -347$ kJ/mol for the reaction of In2O with nitrogen monohydride. In addition to In_2O, indium III oxide - In_2O_3 can also form indium nitride after reaction with NH_2 and NH (Gibbs energies −119 and −263 kJ/mol respectively).

Generally speaking the growth of InN is a challenging task because the equilibrium vapor pressure of nitrogen over InN is quite high and therefore needs the application of low growth temperatures. According to the literature, due to very high activities of ionized precursors, the lowest growth temperatures for InN nanostructures (400–450 ºC) were achieved when applying the plasma-assisted technologies. For example, the indium nitrides with best electronic properties were produced on GaN and AlN buffer layers using plasma-assisted molecular beam epitaxy [31,32,33].

In the most commonly used technologies (chemical vapor deposition, UV-assisted growth, vapor phase epitaxy etc.), which utilize unionized vapor, InN can be produced only at temperatures beginning from 500 ºC [34,35,36]. In these processes the morphology of InN nanostructures mostly depends on the growth temperature, evolving from quantum dot sized nanoparticles formed at 500 ºC, to nanorods grown at 700 ºC [37]. As it is evidenced in Figure 11, in the hydrazine-based technology InN nanoparticles are produced at 450 ºC. This growth temperature is low in comparison with other techniques which use unionized vapor, proving once again that the hydrazine decomposition products have a high activity.

The absence of reliable thermochemical data on $In_2Ge_2O_7$ makes it difficult to determine the possible chemical pathways for the synthesis of indium germinates in our experiments. $In_2Ge_2O_7$ nanostructures are more frequently produced by carbon–assisted thermal evaporation of In_2O_3/GeO_2, In_2O_3/Ge or In/GeO_2 powders at temperatures close to 1000 ºC in the hot zone, and 600 ºC or higher in the cold zone where synthesis takes the place [38–42]. As it was shown, the onset of crystalline $In_2Ge_2O_7$ formation in our technology is close to 450 ºC. This temperature is by 100–150 ºC lower than the growth temperatures reported in literature. The lowering of synthetic temperature in hydrazine-based technology can be again explained by a high activity of N_2H_4 decomposition products.

It should be noted that $In_2Ge_2O_7$ decomposes at and above 700 ºC [43,44]. As a result, the gaseous phase of O_2 and GeO evolve, causing the enrichment of material with In_2O_3. According to this, when pure In and Ge powders were evaporated in O_2+Ar flow, the monoclinic $In_2Ge_2O_7$ was formed at 700 ºC, while at elevated temperatures the Ge doped cubic In_2O_3 was produced [9].

$In_2Ge_2O_7$ nanowires grown by hydrazine-based technology have monoclinic (T-type) structure, as shown in Figure 12 e. Usually, the same monoclinic $In_2Ge_2O_7$ nanomaterials are synthesized and studied in most of experimental works, because a high pressure is needed for the formation of more stabile cubic $In_2Ge_2O_7$ [45,46].

4. Conclusions

The low-temperature technology was developed for the growth of 1D nanostructures, which implies the evaporation of solid sources in the vapor of hydrazine decomposition products at a pressure of 10 Torr. Hydrazine was diluted with water (3 mol.%), which served for producing volatile suboxides on the source surfaces and their subsequent transfer to the substrate, located in the cold zone of a quartz reactor.

α-Ge_3N_4 nanowires and nanobelts were produced directly on Ge source surface at 500 and 520 ºC respectively. After condensation of volatile GeO suboxides onto Si substrate placed in the cold-zone (480 ºC), the chain like non-crystalline Ge microstructures and droplets were produced due to the reduction of GeO in hydrazine vapor. Further increase of Si temperature up to 500 ºC caused the formation of a mixture of Ge chains and tapered α-Ge_3N_4 nanowires grown through the

self-catalyzed VLS method. At 520 ºC, only crystalline germanium nitride was produced on Si substrate. The growth temperature of Ge_3N_4 micro- and nanostructures in hydrazine vapor was reduced by 350 ºC in comparison with data, presented in literature.

Annealing of Ge+In source in hydrazine vapor at 400 ºC caused the formation of tapered In_2O_3 nanowires on the Si substrate. The increase of temperature up to 450 ºC caused dramatic changes in process chemistry. As a result, the nanowires of wide gap $In_2Ge_2O_7$ with attached InN nanocrystals were produced on Si substrate. The growth temperatures of both, $In_2Ge_2O_7$ and InN nanostructures were by 50–150 ºC lower than that, reported in the literature.

The decrease of nitride and oxide nanowire growth temperatures in the developed hydrazine-based technology can be explained by a high activity of products, formed after pyrolytic decomposition of hydrazine. We suppose that in spite of low lifetime of active NH and NH_2 radicals, they play a pivotal role in the synthesis of nitrides, reduction of oxides and formation of volatile molecules. Together with other hydrazine decomposition products, they provide means for lowering the nanostructure growth temperature. The results of this work clearly show that the hydrazine–based technology can serve as a platform for the development of low-temperature technologies, which will be aimed at the growth of different nitride and oxide nanomaterials, including wide bandgap nanostructures.

Conflict of Interest

The authors declare no conflicts of interest regarding this paper.

References

1. Tian W, Lu H, Li L (2015) Nanoscale ultraviolet photodetectors based on one-dimensional metal oxide nanostructures. *Nano Res* 8: 382–405.
2. Liao M, Koide Y, Sang L (2014) Nanostructured Wide-bandgap Semiconductors for Ultraviolet Detection. *Austin J Nanomed Nanotechnol* 2: 1–2.
3. Sang L, Liao M, Sumiya M (2013) A Comprehensive Review of Semiconductor Ultraviolet Photodetectors: From Thin Film to One-Dimensional Nanostructures. *Sensors* 13: 10482–10518.
4. Tsai1 DS, Lien WC, Lien DH, et al. (2013) Solar-Blind Photodetectors for Harsh Electronics. *Sci Rep* 4: 2628.
5. Zhai T, Fang X, Liao M, et al. (2009) A Comprehensive Review of One-Dimensional Metal-Oxide Nanostructure Photodetectors. *Sensors* 9: 6504–6529.
6. Berardan D, Guilmeau E, Maignan A, et al. (2008) In_2O_3:Ge, a promising n-type thermoelectric oxide composite. *Solid State Commun* 146: 97–101.
7. Chen D, Zhang X, Lee AF (2015) Synthetic strategies to nanostructured photocatalysts for CO_2 reduction to solar fuels and chemicals. *J Mater Chem A* 3: 14487–14516.
8. Liu Q, Zhou Y, Mae et al. (2012) Synthesis of highly crystalline $In_2Ge_2O_7$ (En) hybrid sub-nanowires with ultraviolet photoluminescence emissions and their selective photocatalytic reduction of CO_2 into renewable fuel. *RSC Adv* 2: 3247–3250.
9. Kim SS, Park JY, Kim HS, et al. (2011) Temperature-controlled synthesis of $In_2Ge_2O_7$ nanowires and their photoluminescence properties. *J Phys D Appl Phys* 44: 025502.
10. Jin C, Park S, Kim I, et al. (2014) Enhanced H_2S gas-sensing properties of Pt- functionalized $In_2Ge_20_7$ nanowires. *Appl Phys A* 114: 591–595.

11. Gonkalves AP, Godart C (2014) New promising bulk thermoelectrics: intermetallics, pnictides and chalcogenides. *Eur Phys J B* 87: 42.
12. Combe E, Bhame SD, Guilmeaua E, et al. (2012) Synthesis of $In_{2-x}Ge_xO_3$ nanopowders for thermoelectric applications. *J Mater Res* 27: 500–505.
13. Li L, Lee PS, Yan C, et al. (2010) Ultrahigh-Performance Solar-Blind Photodetectors Based on Individual Single-crystalline $In_2Ge_2O_7$ Nanobelts. *Adv Mater* 22: 5145–5149.
14. Kong XY, Ding Y, Yang R, et al. (2004) Single-Crystal Nanorings Formed by Epitaxial Self-Coiling of Polar Nanobelts. *Science* 303: 1348–1351.
15. Kirkham M, Wang ZL, Snyder RL (2008) In situ growth kinetics of ZnO nanobelts. *Nanotechnology* 19: 445708.
16. Pan ZW, Dai ZR, Wang ZL (2001) Nanobelts of semiconducting oxides. *Science* 291: 1947–1949.
17. Vashioka S, Tokaynagi S (1967) Deposition of silicon nitride films by the silicon hydrazine process. *J Electrochem Soc* 114: 962–963.
18. Rzhanov AV (1982) Silicon nitride in electronics. Novosibirsk: Nauka, 200.
19. Santos LB, Ribeiro CA, Capela JMV, et al. (2013) Kinetic parameters for thermal decomposition of hydrazine. *J Therm Anal Calorim* 113: 1209–1216.
20. Pakdehi S, Salim M, Rasoolzadeh M (2014) A Review on Decomposition of Hydrazine and Its Kinetics as a Novel Approach for CO-Free H_2 Production. *Res Appl Mech Eng* 3: 21–25.
21. Dirtu D, Odochian L, Pui A, et al. (2006) Thermal decomposition of ammonia. N_2H_4-an intermediate reaction product. *Centr EurJ Chem* 4: 666–673.
22. Jishiashvili D, Shiolashvili Z, Makhatadze N, et al. (2015) Vapor-Solid growth of InP and Ga_2O_3 based composite nanowires. *Eur Chem Bull* 4: 24–29.
23. Jishiashvili D, Kiria L, Shiolashvili Z, et al. (2013) Formation of Germanium Nitride Nanowires on the Surface of Crystalline Germanium. *J Nanosci* 2013: 10.
24. Saleem U, Wang H, Peyrot D, et al. (2016) Germanium-catalyzed growth of single-crystal GaN nanowires. *J Cryst Growth* 439: 28–32.
25. Jumidali MM, Hashim MR, Sulieman KM (2010) Germanium catalyzed amorphous silicon dioxide nanowire synthesized via thermal evaporation method. International Conference on Enabling Science and Nanotechnology (ESciNano), Kuala Lumpur (1–3 Dec. 2010): 1–2.
26. Pan ZW, Dai Sh, Rouleau CM, et al. (2005) Germanium-Catalyzed Growth of Zinc Oxide Nanowires: A Semiconductor Catalyst for Nanowire Synthesis. *Angewandte Chem* 117: 278–282.
27. Gu Z, Liu F, Howe JY, et al. (2009) Germanium-catalyzed hierarchical Al_2O_3 and SiO_2 nanowire bunch arrays. *Nanoscale* 1: 347–354.
28. Mullin JW (2001) Crystallization. Woburn: Reed Edu. & Prof. Publ. Ltd.
29. Gao YH, Bando Y, Sato T (2001) Nanobelts of the dielectric material Ge_3N_4. *Appl Phys Lett* 79: 4565–4567.
30. Xie T, Jiang Z, Wu G, et al. (2005) Characterization and growth mechanism of germanium nitride nanowires prepared by an oxide-assisted method. *J Cryst Growth* 283: 286–290.
31. Stoica T, Meijers R, Calarco R, et al. (2006) MBE growth optimization of InN nanowires. *J Cryst Growth* 290: 241–247.
32. Denker C, Malindretos J, Werner F, et al. (2008) Self-organized growth of InN-nanocolumns on p-Si(111) by MBE. *Phys Stat Solidi (C)* 5: 1706–1708.
33. Goff LE, Powell REL, Kent AJ, et al. (2014) Molecular beam epitaxy of InN nanorods on Si- and C-faces of SiC substrates. *J Cryst Growth* 386: 135–138.

34. Cai ZM, Ye F, Jing SY, et al. (2008) A systematic study of chemical vapor deposition growth of InN. *Appl Surf Sci* 255: 2153–2158.
35. Kao M, Erasmus RM, Moloto N, et al. (2015) UV-assisted synthesis of indium nitride nano and microstructures. *J Mater Chem A* 3: 5962–5970.
36. Rafique S, Han L, Zhao H (2015) Chemical vapor deposition of m-plane and c-plane InN nanowires on Si (100) substrate. *J Cryst Growth* 415: 78–83.
37. Madapu KK, Dhara S, Polaki S, et al. (2015) Growth of InN quantum dots to nanorods: a competition between nucleation and growth rates. *Cryst Eng Comm* 17: 3139–3147.
38. Tian W, Zhi C, Zhai T, et al. (2012) Ultrahigh quantum efficiency of CuO nanoparticle decorated $In_2Ge_20_7$ nanobelt deep-ultraviolet photodetectorst. *Nanoscale* 4: 6318–6324.
39. Liu Z, Huang H, Liang B, et al. (2012) Zn_2GeO_4 and $In_2Ge_2O_7$ nanowire mats based ultraviolet photodetectors on rigid and flexible substrates. *Opt Express* 20: 2982–2991.
40. Yan C, Singh N, Lee PS (2009) Morphology Control of Indium Germanate Nanowires, Nanoribbons and Hierarchical Nanostructures. *Cryst Growth Design* 9: 3697–3701.
41. Chaoyi Y, See LP (2010) Synthesis of One-dimensional (ID) Ge-based Ternary Oxide Nanostructures. *Nanoelectronics Conference (I NEC*) Hong Kong: 408–409.
42. Zhan J, Bando Y, Hu J, et al. (2006) Hollow and polygonous microtubes of monocrystalline Indium Germanate. *Angew Chem Int Ed* 45: 228–231.
43. Bukowski TJ (2002) The optical and photoconductive response in germanium quantum dots and indium tin oxide composite thin film structures. *Thesis.* University of Florida.
44. Sarkisov PD (1971) *Neorg Mater* 7: 341–345.
45. Karazhanov SZ, Ravindran P, Grossner U (2011) First-principles study on electronic structure, phase stability, and optical properties of $In_2X_2O_7$ (X═C, Si, Ge or Sn). *Thin Solid Films* 519: 6561–6567.
46. Li H, Li Y, Li N, et al. (2015) A comparative study of high pressure behaviors of pyrochlore-type and thortveitite-type $In_2Ge_2O_7$. *RSC Adv* 5: 44121–44127.